Aust. J. Phys., 1990, **43**, 779–91

A Tomographic Investigation of Variations in the Excited State Populations of $\boldsymbol{E} \times \boldsymbol{B}$ Discharges

A. M. Garvie[A] *and M. J. Brennan*[B]

Institute for Atomic Studies, Flinders University of South Australia, Bedford Park, S.A. 5042, Australia.
[A] Present address: Weber Research Institute, Polytechnic University, Route 110, Farmingdale, NY 11735, U.S.A.
[B] Present address: Atomic and Molecular Physics Laboratories, Research School of Physical Sciences, Australian National University, G.P.O. Box 4, Canberra, A.C.T. 2601, Australia.

Abstract

A comparison of the spatial distribution of emissions from two molecular nitrogen electronic states of markedly different threshold energies has been made in a non self-sustained Townsend discharge in an $\boldsymbol{E} \times \boldsymbol{B}$ field. The spatial mapping has been performed using a combination of the 'photon flux' technique and reconstructive tomography. Observed differences in the spatial distribution of the two excited states are interpreted in terms of the gradient expansion of the energy distribution function. Comparisons made with the results of two-model simulations confirm this interpretation.

1. Introduction

The work presented here is an extension of investigations of discharge characteristics reported in a companion paper (Brennan and Garvie 1990; present issue p. 765). That paper, from here on referred to as BG, reports the experimental determination of transport parameters and their application to the evaluation of a model for an $\boldsymbol{E} \times \boldsymbol{B}$ discharge in molecular nitrogen.

In the present paper the experimental apparatus reported in BG is used to examine spatial variations of the ratio of excited states for the $C^3\Pi_u$ to $B^3\Pi_g(0\text{–}0)$ transition at $337 \cdot 1$ nm and the $B^2\Sigma_u^+$ to $X^2\Sigma_g^+(0\text{–}0)$ transition at $391 \cdot 4$ nm in an $\boldsymbol{E} \times \boldsymbol{B}$ discharge. The threshold energies for excitation to the $C^3\Pi_u$ and the $B^2\Sigma_u^+$ states are $11 \cdot 03$ and $18 \cdot 75$ eV respectively. As indicated by Brennan *et al.* (1990), observation of these two lines effectively probes different parts of the electron energy distribution. Interpretation is made via the gradient expansion of the energy distribution function. A similar study in the absence of a magnetic field has been made by Wedding and Kelly (1989). In that case the steady stream discharge was radially symmetric about an axis in the electric field direction and the spatial distribution of excited states could be determined using the Abel inversion. The application of a perpendicular magnetic field brings about a loss of axial symmetry and consequently the spatial variation of excited states must be determined from the more general and complex Radon inversion. Such measurements have the potential to provide a sensitive test of the hydrodynamic theory and gas models. Comparison with Monte Carlo simulations by using two different cross-section sets for nitrogen illustrates this point.

0004-9506/90/060779$03.00

2. Tomography: A Means of Spatial Mapping

The spatial variation of photons emitted from decaying molecular excited states in a discharge can be determined generally using the Radon and inverse Radon transforms coupled with an appropriate experiment. This is well established and demonstrated in the field of tomography, which provides techniques for determining the distribution of a parameter in three-dimensional space without disruption of the distribution. A knowledge of the 'line integrals' of the parameter has been shown by Radon (1917) and Dean (1983) to be adequate for mapping the two-dimensional distribution, say $f(x, y)$, in a particular z plane of an object. Stacking a set of z planes produces a reconstruction of the three-dimensional distribution.

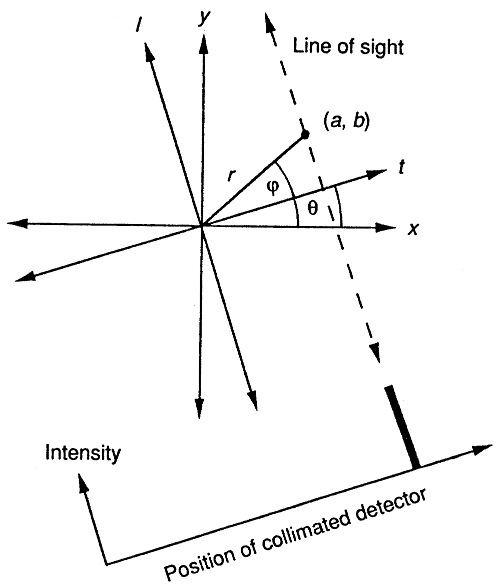

Fig. 1. Illustration of the line of sight at angle θ for an object located at (r, ϕ) in the coordinate system (x, y) of the discharge, and its relationship to the rotating collimated detector axes (t, l).

In the present experiment the distribution to be reconstructed is the excited state distribution for specific states. 'Line integrals' of the emitted photons are determined using the single photon detection system described in BG, which has a well collimated line of sight. An understanding of the reconstruction process is obtained by considering photon emission from a point, say (a, b), fixed within a coordinate system (x, y), as indicated in Fig. 1, and producing unfiltered reconstructions.

A second cartesian coordinate system (t, l), which is a rotation of the (x, y) system through angle θ, is introduced and a detector of parallel line integrals, a collimator and photomultiplier in this case, is located away from the object and orthogonal to the l axis. The measured photon flux originating from a source at (a, b), fixed with respect to the (t, l) system, is

$$p(t, \theta) = \int_{-\infty}^{+\infty} f(t, l)\, \mathrm{d}l, \tag{1}$$

where f is the excitation rate at (t, l) and the $p(t, \theta)$ is referred to as the Radon transform or projection data. An approximate image of the spatial distribution of excited states is obtained by measuring sets of $p(t,\theta)$ for a large number of angles and then performing the approximate inverse operation of summing back-projections. The back-projection operation involves drawing a line along each path in the image plane corresponding to a line of integration in the object plane. The intensity of the back-projected line is represented by the value of $p(t,\theta)$. For the case of a point source only, for example, one line is drawn at each angle and the intensity of all lines is the same, that is, $p(t,\theta)$ is independent of angle. Integrating all back-projections at correct orientations produces the summation back-projection

$$\tilde{f}(x, y) = \int_0^{\pi} p(t, \theta)\, \mathrm{d}\theta . \tag{2}$$

Performing the integration shows that

$$\tilde{f}(x, y) = \frac{f(a, b)}{\{(x-a)^2 + (y-b)^2\}^{\frac{1}{2}}} = \frac{f(a, b)}{R}, \tag{3}$$

where R is the distance between points (x,y) and (a,b) (Vainshtein 1971). For a finite number of angles the integration in equation (2) is approximated by a summation and results in a star-like pattern, as illustrated in Fig. 2. It is obvious from equation (3) and Fig. 2 that the summation back-projection is not a perfect representation of $f(x,y)$. Nonzero contributions due to a point at $\boldsymbol{r} = (a,b)$ occur at locations $\boldsymbol{r}' = (x,y)$ in the image plane. For back-projections at all angles, θ: $0 \leq \theta < \pi$, the contribution at a point $\boldsymbol{r}'$ is inversely proportional to the distance between $\boldsymbol{r}$ and $\boldsymbol{r}'$. Equation (2) is linear and hence the summation back-projection for many sources is the same as the sum of summation back-projections of individual sources. Thus, the image of many sources will contain blurring contributions from all sources and consequently is a poor representation of the discharge. Removal of this blur is necessary to determine the shift in the spatial locations of the two excited states.

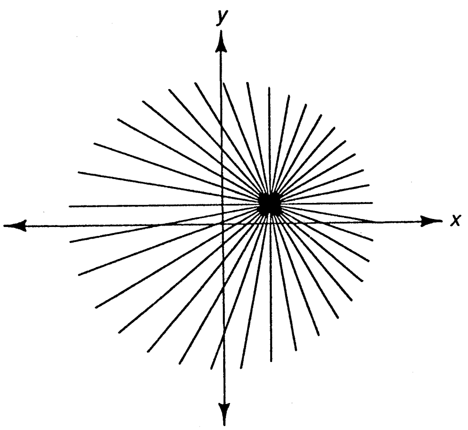

Fig. 2. An unfiltered summation back-projection reconstructed from data collected at 18 equally space viewing angles from a point object located in the first quadrant. This type of reconstruction produces an image that contains $1/R$ like blurring.

Application of the inverse Radon transform,

$$f(r, \phi) = \frac{1}{4\pi^2} \int_0^{2\pi} \int_{-\infty}^{+\infty} - \frac{1}{t - r\cos(\theta-\phi)} \frac{\mathrm{d}p(t, \theta)}{\mathrm{d}t}\, \mathrm{d}t\, \mathrm{d}\theta ,$$

where $p(t, \theta)$ is the projection data at angle θ, eliminates the blur. This transform reconstructs an image from a complete set of projection data assuming the distribution $f(r, \phi)$ is bounded, continuous and zero outside the region being scanned, and that the partial derivative of $p(t, \theta)$ with respect to t is continuous.

In digital applications the transform has been implemented in numerous ways. Two major categories are iterative (also known as algebraic) and analytic reconstruction (Dean 1983; Brooks and Di Chiro 1976; Herman 1980). The technique selected for application in this study was the analytical reconstruction method, known as convolution filtering.

Insight into how the inverse Radon transform can be applied to the problem is gained by considering an equivalent equation developed by Bracewell and Riddle (1967); where the Radon transform is

$$p(t, \theta) = \int_{-\infty}^{+\infty} \int_{-\infty}^{+\infty} f(x, y)\, \delta(x \cos\theta + y \sin\theta - t)\, \mathrm{d}x\, \mathrm{d}y,$$

it is possible to determine $f(x, y)$ from a complete set of Radon transforms and

$$f(x, y) = \int_0^{\pi} h(t, \theta)\, \mathrm{d}\theta, \tag{4}$$

where

$$h(t, \theta) = \int_{-\infty}^{+\infty} p(T, \theta)\, k(t - T)\, \mathrm{d}T, \tag{5}$$

$$k(t) = 2M^2 \operatorname{sinc}(2Mt) - M^2 \operatorname{sinc}^2(Mt). \tag{6}$$

Here M is the spatial frequency equal to the highest Fourier component of $p(t, \theta)$ (i.e. M is the Nyquist limit) and $\operatorname{sinc} x = (\sin \pi x)/\pi x$. These equations assume that the projection data are continuous in t and θ. However, in experiments the projection data are sampled at a finite number of points and a finite number of projections are measured. As a result of this sampling the distribution cannot be reconstructed exactly. Although $f(x, y)$ is no longer determined perfectly, it is well established that good approximations are attainable (Brooks and Di Chiro 1976).

To apply the reconstruction method experimentally it is necessary to obtain a discrete approximation to the filter function (6). One method of doing this is to assume that the individual elements of the projection data are of width a and have zero separation. As a result of this t is replaced by na and M by $1/2a$, so that the expression for the filter function becomes

$$k(na) = 2\left(\frac{1}{2a}\right)^2 \operatorname{sinc} n - \left(\frac{1}{2a}\right)^2 \operatorname{sinc}^2\left(\frac{n}{2}\right),$$

i.e.

$$k(na) = \begin{cases} 1/4a^2 & \text{for } n = 0 \\ -1/(\pi n a)^2 & \text{for } n \text{ odd} \\ 0 & \text{for } n \text{ even}, \end{cases} \tag{7}$$

where n takes both positive and negative integer values.

These values can be used to obtain a discrete approximation to the filtered projection data described by (5):

$$h(na, \theta_j) = a \sum_{m=-\infty}^{+\infty} p(ma, \theta_j)\, k((m-n)a),$$

which after substitution of (7) becomes

$$h(na, \theta_j) = p(na, \theta_j)/4a - (1/a\pi^2) \sum_{i \text{ odd}} p((n+i)a)/i^2 .$$

Correspondingly, the approximation to (4) is

$$f(x, y) = \sum_j h(na, \theta_j)\Delta\theta .$$

3. Reconstruction from Transverse Scans

It is clear that the spatial resolution of the reconstructed images of the photon count rates is dependent on the number of viewing angles in the range $0 \leq \theta < \pi$, and the number of line of sight integrals measured at each angle. The experimental apparatus, described in BG, was constructed with the capability of changing the viewing angle of the collimated detector with respect to the magnetic field. This allowed measurements of the photon flux to be made at several points orthogonal to the electric field to characterise the profile of the discharge at a selected angle. Several such transverse scans were made at up to five 'z positions' between the anode and the cathode. Although tomographic reconstruction generally requires viewing angles between 0 and 180°, the symmetry of the discharge about a plane orthogonal to both applied fields (see BG) allows the angular range of data collection to be reduced to 90°.

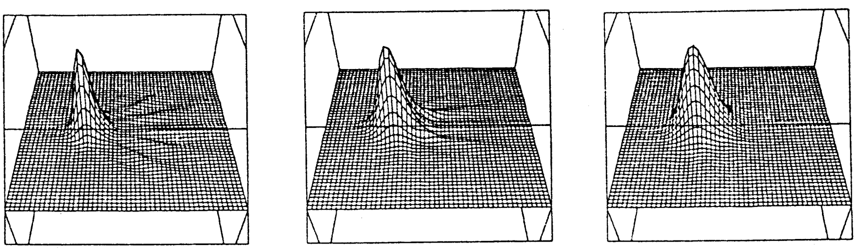

(*a*) (*b*) (*c*)

Fig. 3. Tomographic reconstructions of the full spectral emission of an $\boldsymbol{E}\times\boldsymbol{B}$ discharge in molecular nitrogen ($E/N = 465$ Td and $B/N = 561\times10^{-17}$ G cm^3) at distances (*a*) $z = 0 \cdot 31$ cm, (*b*) $z = 0 \cdot 61$ cm and (*c*) $z = 0 \cdot 91$ cm from the cathode. The $\boldsymbol{E}\times\boldsymbol{B}$ drift is responsible for the shift of the main body of the discharge along the positive x axis (i.e. to the right) with increasing z and the broadening is due to diffusion.

Data were measured at six viewing angles over this reduced range. After measurement, each transverse scan was fitted to a function, the sum of two gaussians, allowing normalisation and interpolation of the count rates between data points. The expectation that the electron number density in any x–y

plane is a smoothly varying function justifies cubic spline interpolation of the projection data as a function of angle. From this and the assumption of symmetry about the $y=0$ plane, data were obtained to produce reconstructions on a 51×51 grid in the x–y plane from 51 viewing angles. Fig. 3 is a series of reconstructions of photon emission integrated over the flux from all states, i.e. with no interference filters for state selection, for a typical steady stream discharge at distances of 0·31, 0·61 and 0·91 cm from the cathode. The increasing displacement of the centroid of the stream to the right, along the x axis, due to $\boldsymbol{E}\times\boldsymbol{B}$ drift and the broadening due to diffusion with increasing z displacement are easily seen.

Fig. 3 demonstrates that the photon flux technique combined with tomographic reconstruction provides a means of mapping the spatial variation of photon emission. It should be noted that the plotting routine has normalised the plots at the peak value and that small amplitude ridges in the reconstruction are due to uncertainties in determining the position of the projection of the axis of rotation of the prism onto the transverse scan data.

4. Spatial Variations in the Excitation Rate

The spatial variation in the excited state population in a steady state discharge is related to the distribution function f_0 by

$$n(x,y,z)\,\nu_{(l)}(x,y,z)=\left(\frac{2}{m}\right)^{\frac{1}{2}}N\int_0^\infty Q_{(l)}\,\epsilon^{\frac{1}{2}}f_0(x,y,z,\epsilon)\,\mathrm{d}\epsilon\,,$$

where $Q_{(l)}$ is the cross section for excitation to the lth state and N is the background gas number density. Making a gradient expansion of f_0 demonstrates the spatial dependence of the excitation rates:

$$n(x,y,z)\nu_{(l)}(x,y,z)=n(x,y,z)\left(\nu_{(l)}^{000}-\nu_{(l)}^{100}\frac{1}{\lambda_z n}\frac{\partial n}{\partial x}-\nu_{(l)}^{001}\frac{1}{\lambda_z n}\frac{\partial n}{\partial z}\right), \tag{8}$$

to the first order in derivatives in n, where

$$\nu_{(l)}^{ijk}=\left(\frac{2}{m}\right)^{\frac{1}{2}}N\int_0^\infty Q_{(l)}\,\epsilon^{\frac{1}{2}}g^{ijk}(\epsilon)\,\mathrm{d}\epsilon\,. \tag{9}$$

Here $\nu_{(l)}^{000}$ is the swarm averaged excitation rate, $\lambda_z=W_z/2D_z$ and $(1/\lambda_z\,n)\partial n/\partial z$ is of the order of the ratio of the drift flux to the diffusion flux. The $g^{ijk}(\epsilon)$, arising from the gradient expansion of f_0, are defined in Brennan *et al.* (1990). An alternative expression to (8) is

$$n(x,y,z)\,\nu_{(l)}(x,y,z)=\nu_{(l)}^{000}\left(n(x,y,z)-\frac{\nu_{(l)}^{100}}{\nu_{(l)}^{000}}\frac{1}{\lambda_z}\frac{\partial n}{\partial x}-\frac{\nu_{(l)}^{001}}{\nu_{(l)}^{000}}\frac{1}{\lambda_z}\frac{\partial n}{\partial z}\right)$$

and for small $(1/\lambda_z)\partial n/\partial x$ and $(1/\lambda_z)\partial n/\partial z$ this can be written as

$$n(x,y,z)\,\nu_{(l)}(x,y,z)=\nu_{(l)}^{000}\,n(x-\Delta x,y,z-\Delta z)\,,$$

where

$$\Delta x=\frac{1}{\lambda_z}\frac{\nu_{(l)}^{100}}{\nu_{(l)}^{000}}\quad\text{and}\quad\Delta z=\frac{1}{\lambda_z}\frac{\nu_{(l)}^{001}}{\nu_{(l)}^{000}}\,.$$

From this we can interpret the total excitation rate at (x, y, z) to be equal to the swarm averaged excitation rate multiplied by the number of electrons at a position slightly shifted in x and z, as in Brennan *et al.* Measurement of the excited state density as a function of position (x, y, z) for two different states, such as the $B^2\Sigma_u^+$ and $C^3\Pi_u$, yields a measure of the validity of the gradient expansion and the importance of various terms in the expansion for the description of the discharge.

The Monte Carlo simulation studies of Brennan *et al.* (1990) demonstrated that terms involving the the first order derivative in x, and hence Δx, may be ignored for the conditions studied, at least in the case of transport parameter determination from measurements of the total photon flux. Let us assume for a moment that this approximation is valid when considering the spatial variation of the photon flux from two arbitrary states, say 1 and 2, in a steady stream discharge. The excited state distribution for the state 1 in the $y = 0$ plane is

$$\mathcal{N}_{(l)}(x, 0, z) = k_{(l)}\, n(x, 0, z)\left(\nu_{(l)}^{000} - \frac{1}{\lambda_z n}\frac{\partial n}{\partial z}\,\nu_{(l)}^{001}\right) \tag{10}$$

to first order in $\partial n/\partial z$, where $k_{(l)}$ is a measure of the detection efficiency of radiation from the lth state.

Integrating (10) over x and y within the steady state Townsend region we obtain the total number of excited states at z:

$$\mathcal{N}_{(l)}(z) = k_{(l)}\, n'(z)\left(\nu_{(l)}^{100} - \frac{\alpha_T}{\lambda_z}\,\nu_{(l)}^{001}\right).$$

Normalising (10) to the total number of excited states at z eliminates the experimental efficiency factor $k_{(l)}$:

$$\frac{\mathcal{N}_{(l)}(x, 0, z)}{\mathcal{N}_{(l)}(z)} = \frac{n(x, 0, z)}{n'(z)}\left(\nu_{(l)}^{000} - \frac{1}{\lambda_z n}\frac{\partial n}{\partial z}\,\nu_{(l)}^{001}\right)\Big/\left(\nu_{(l)}^{000} - \frac{\alpha_T}{\lambda_z}\,\nu_{(l)}^{001}\right). \tag{11}$$

Taking the ratio of similar expressions for two arbitrary states removes the need to determine the electron number density and provides the expression

$$\frac{\mathcal{N}_1(x, 0, z)/\mathcal{N}_1(z)}{\mathcal{N}_2(x, 0, z)/\mathcal{N}_2(z)} = \left(1 - \frac{1}{\lambda_z n}\frac{\partial n}{\partial z}\,\nu_1^{001}/\nu_1^{000}\right)\left(1 - \frac{\alpha_T}{\lambda_z}\,\nu_2^{001}/\nu_2^{000}\right)\Big/$$
$$\left(1 - \frac{1}{\lambda_z n}\frac{\partial n}{\partial z}\,\nu_2^{001}/\nu_2^{000}\right)\left(1 - \frac{\alpha_T}{\lambda_z}\,\nu_1^{001}/\nu_1^{000}\right). \tag{12}$$

For conditions where the first order gradient expansion, i.e. (10), is valid, it can safely be assumed that $(\alpha_T/\lambda_z)\nu_{(1)}^{001}/\nu_{(1)}^{000}$ is small. Thus, the binomial expansion of (12) can be used to give the ratio of normalised excited state populations, for the two states, as a function of x and z:

$$\frac{\mathcal{N}_1(x, 0, z)/\mathcal{N}_1(z)}{\mathcal{N}_2(x, 0, z)/\mathcal{N}_2(z)} = 1 - \left(\frac{1}{\lambda_z n}\frac{\partial n}{\partial z} - \frac{\alpha_T}{\lambda_z}\right)\left(\frac{\nu_1^{001}}{\nu_1^{000}} - \frac{\nu_2^{001}}{\nu_2^{000}}\right). \tag{13}$$

This is an approximate representation of (12), equivalent to the result of Wedding and Kelly (1989) for the $B=0$ case. It is important to realise that the assumption that $(\alpha_T/\lambda_z)\nu_{(l)}^{001}/\nu_{(l)}^{000}$ is small is implicit in the assumption that the gradient expansion is valid, and it is here that the comparison with the experiment acts as a test of the validity of the underlying theory. We also note that it is highly desirable to avoid an analysis which requires the determination of the electron number density $n(x,y,z)$, because the presence of ionisation in the discharge *precludes* its determination by indirect means, such as measurement of the discharge current (Blevin and Fletcher 1984). The assumption that the contribution of the terms in $\partial n/\partial x$ is negligibly small, when considering excited state distributions in the manner outlined above, can be investigated using Monte Carlo techniques. Retaining the terms in $\partial n/\partial x$ in the gradient expansion and making a binomial expansion in the same manner as above provides an alternative expression to (13) for the normalised ratio of excited state populations:

$$\frac{\mathcal{N}_1(x,0,z)/\mathcal{N}_1(z)}{\mathcal{N}_2(x,0,z)/\mathcal{N}_2(z)}$$

$$=1-\left(\frac{1}{\lambda_z n}\frac{\partial n}{\partial z}-\frac{\alpha_T}{\lambda_z}\right)\left(\frac{\nu_1^{001}}{\nu_1^{000}}-\frac{\nu_2^{001}}{\nu_2^{000}}\right)-\left(\frac{1}{\lambda_z n}\frac{\partial n}{\partial z}\right)\left(\frac{\nu_1^{001}}{\nu_1^{000}}-\frac{\nu_2^{001}}{\nu_2^{000}}\right). \quad (14)$$

By using the Monte Carlo code of Brennan *et al.* and the cross-section set of Phelps and Pitchford (1985) for nitrogen,* the number of excitations to the $B^2\Sigma_u^+$ and the $C^3\Pi_u$ states were monitored as a function of x and z at $y=0$ in simulations conducted for the experimental conditions discussed in

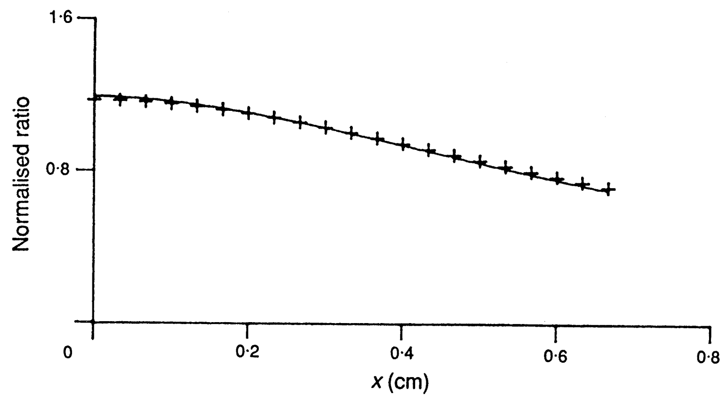

Fig. 4. A comparison of simulated values of the normalised ratio of excited states using two different approximations for the gradient expansion (equations 13 and 14) plotted as a function of x along the line $y=0$ at $z=0\cdot61$ cm. The close agreement between the expressions justifies the use of equation (12) in the analysis of tomographic reconstructions.

* In this work the cross-section sets used in simulations are intended to be 'illustrative', rather than 'definitive' as in BG. It is unlikely that the use of an alternative gas model, such as that by Ohmori *et al.* (1988), would change the general conclusions made here, especially in the light of the reservations about the Ohmori *et al.* set expressed in BG.

the next section. The population of these two states were monitored because they correspond to the upper states of the lines studied experimentally. The x dependence of the two approximations (13) and (14) near the maximum in electron number density is compared in Fig. 4 at an axial position z corresponding to that of the experiment. The close agreement between the two levels of approximation suggests that (12) can be used with confidence in the analysis of the experiment under similar conditions, confirming the analysis used in BG.

5. Experimental Results

Reconstructive tomography of the photon flux from a discharge requires a relatively large number of measurements to determine the photon flux 'profile' from several angles. As mentioned in the introduction, the experimental apparatus described in BG was used. Narrow band interference filters were placed between the collimator viewing the discharge and the photomultiplier in order to select the radiation due to single transitions only. The lines studied were the (0–0) transition for $C^3\Pi_u$ to $B^3\Pi_g$ (337·1 nm) and the $B^2\Sigma_u^+$ to $X^2\Sigma_g^+$(0–0) transition (391·4 nm). Competing phenomena constrained the choice of operating conditions for the tomographic measurements, which required stable discharge conditions with significant photon flux from the channels monitored, over the 4–5 hour experimental runs. This demanded a compromise between the experimental parameters E/N, the reduced electric field, and the applied magnetic field B. In order to measure a difference in the distribution of photons from the two excited states, a relatively high applied magnetic field was required to obtain a sufficiently large displacement of the swarm in the $\boldsymbol{E}\times\boldsymbol{B}$ direction with respect to the position between the electrodes. However, simulations conducted using the three cross-section sets mentioned in BG (i.e. those of Tagashira *et al.* 1980; Phelps and Pitchford 1985; Ohmori *et al.* 1988), all confirm that an increase in the magnetic field strength, for a given E/N, results in a reduction in the mean energy of the discharge, with a corresponding drop in excitation to the 'probe states' and less ionisation. In principle this effect can be compensated for by increasing the number of injected electrons by applying more power to the electron source, an oxide coated cathode. The efficacy of this remedy was limited by the increasing oxidation/degradation of the electron source by gas impurities in operation, at the relatively high pressures used. In any case, the acknowledged limitations of the gas models mentioned above in predicting ionisation growth prohibit a precise optimisation of the experimental conditions through extensive preliminary simulations.

Experience gained in the course of the BG measurements and through the simulation studies resulted in the experimental parameters $E/N = 465$ Td and $B/N = 561\times10^{-17}$ G cm^3 in 0·75 Torr of nitrogen (normalised to 0°C) being chosen for the tomographic study, given the constraints discussed above. The measurements for the tomograms for each line were made at a distance 0·61 cm from the cathode where the discharge amplification, due to ionisation, made the relatively low photon count rates for both probe channels acceptable from a statistical standpoint. These measurements were repeated again at a distance 0·7 cm from the cathode in a separate experiment. In a similar manner to BG, scans of the 'line of sight' photon flux were made at discrete positions, transverse to the discharge, at six angular positions equispaced between 0 and $\pi/2$ about the electrode symmetry axis. These data formed the basis for the back-projections [$p(t,\theta)$ in equation (5)] required in the analysis. The techniques of BG were used to analyse the profiles taken at 0 and $\pi/2$ radians with respect to the magnetic field and from this analysis the parameters α_T and λ_z of equation (13) were obtained.

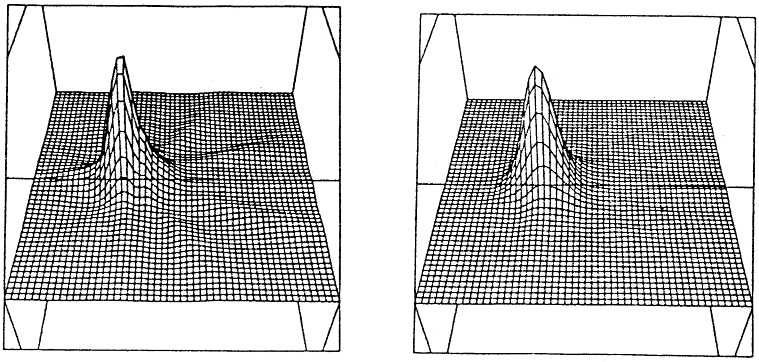

(*a*) (*b*)

Fig. 5. Tomographic reconstructions of a steady state discharge at $z = 0 \cdot 61$ cm for radiation from the (*a*) $B^2\Sigma_u^+$ and (*b*) $C^3\Pi_u$ states.

Tomographic reconstructions of the excitation rates for the $B^2\Sigma_u^+$ and $C^3\Pi_u$ states are shown in Figs 5*a* and 5*b*. The small number of counts for the reconstruction of the $B^2\Sigma_u^+$ state emission is responsible for the deviation from a smooth curve. Efforts were made to obtain a larger sample for this reconstruction. However, this was curtailed by the low count rate combined with the restrictive lifetime of the electron source.

Fig. 6 shows the two excited state populations at $y = 0$, the line about which the discharge is symmetric, derived from the reconstructed tomograms. The shift between the two states is small, approximately 1 mm, with emissions from the $C^3\Pi_u$ state (solid curve) being further to the right than those of the $B^2\Sigma_u^+$ state. This is consistent with the $B^2\Sigma_u^+$ state having a larger shift Δz than the $C^3\Pi_u$ state, because the electrons at the front of the swarm are in general of higher energy than those at the rear for an isolated swarm. In Fig. 7 the ratio of the two normalised states is compared with the fitted ratio obtained using (12) at locations where the electron number density is significantly larger than zero. The fitted parameters were offset by Δx, allowing for a non-equilibrium region and uncertainty in the electron source position, ν_B^{001}/ν_B^{000} and ν_C^{001}/ν_C^{000}. Data collection, reconstruction and fitting were performed twice for identical experimental conditions and two positions in the gap, firstly for $z = 0 \cdot 61$ cm and again at $z = 0 \cdot 7$ cm as mentioned above.

In order to gain a better understanding of the experimental results, the difference between the ratio of excited states was also determined from Monte Carlo simulations, similar to those described in BG using the models of Tagashira *et al.* (1980) and Phelps and Pitchford (1985). These models are significantly different, but have been shown to be useful in highlighting experimental features which are sensitive to the gas model used (Kelly *et al.*

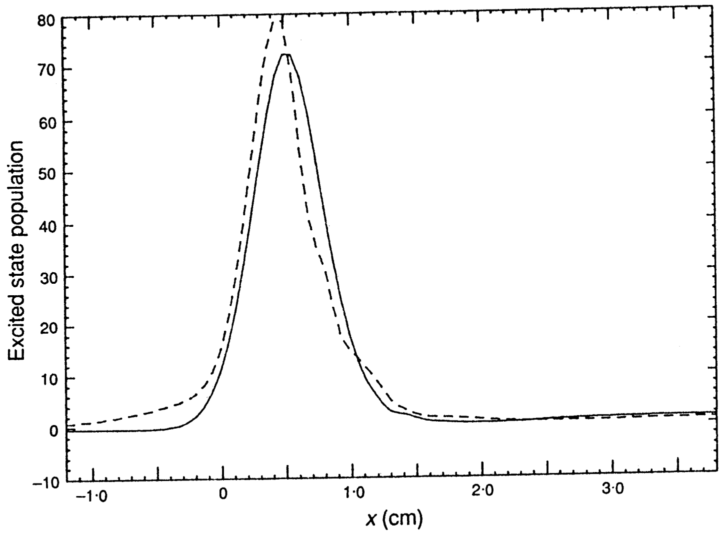

Fig. 6. Excited state populations $B^2\Sigma_u^+$ (dashed curve) and $C^3\Pi_u$ (solid curve) sampled along the symmetry line ($y = 0$) in the discharge. The axial position z is $0 \cdot 61$ cm.

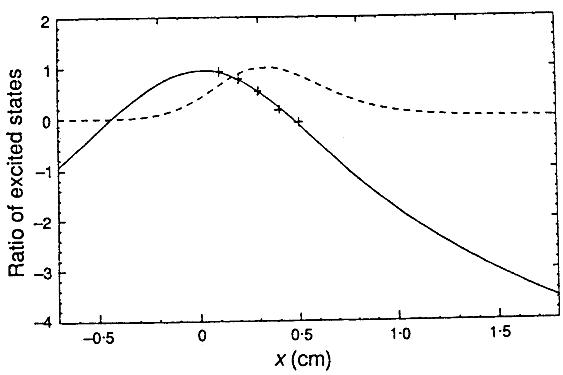

Fig. 7. Deviation of the ratio of excited states from unit: the crosses are experimental values and the solid curve was calculated using equation (12). These are compared with the normalised electron number density (dashed curve) for the line $y = 0$, $z = 0 \cdot 61$ cm.

1989). To assist this study, the cross-section set of Tagashira *et al.* was modified by splitting the single ionisation cross section into cross sections for molecular ionisation, dissociative ionisation (Kunhardt, personal communication 1983) and an excitation to the $B^2\Sigma_u^+$ state (Stanton and St. John 1969). When using the cross sections of Phelps and Pitchford, the cross section of Stanton and St. John for excitation to the $B^2\Sigma_u^+$ state was separated from the total ionisation cross section. Table 1 provides a summary of the results of simulation and experiment.

Table 1. Differences between ratio of excited states

Estimate	$\nu_{\mathrm{B}}^{001}/\nu_{\mathrm{B}}^{000}-\nu_{\mathrm{C}}^{001}/\nu_{\mathrm{C}}^{000}$
Experiment 1	0·5
Experiment 2	2·7
Tagashira *et al.* (1980)	1·05
Phelps and Pitchford (1985)	1·14

Due to its complicated nature, no error analysis of the tomographic reconstruction was undertaken. However, tests of the reconstruction program made in the context of other work (Garvie and Sorell 1990), but not presented here, have demonstrated the program integrity. Also a typical transverse scan used in the reconstruction was of the same quality as those presented in BG and a similar χ^2 fitting technique was used to determine both the transport parameters and the ratio of excited states.

6. Conclusions

Tomographic reconstructions of photon emission from a steady stream Townsend discharge in an $\boldsymbol{E}\times\boldsymbol{B}$ field in nitrogen reveal that the population densities for states with different excitation thresholds have a different spatial dependence. This is consistent with a description of the discharge based on a gradient expansion of the electron energy distribution function. As stated by Wedding and Kelly (1989), such experiments provide explicit evidence for the importance of various terms in the gradient expansion formulation, whereas experiments such as those presented in BG measuring only the electron transport parameters have an implicit dependence only on the validity of gradient expansion.

It is interesting to comment further on the results presented in Table 1. Both of the Monte Carlo simulations, using markedly different gas models, predict that the difference between the ratios for the two states is of the order of unity. The uncertainties involved in the present experiments, reflected in the values 0·5 and 2·7 for the ratio, allow us to say no more than 'this is consistent with experiment'. This result, considered in conjunction with the definition of excitation rate (9), supports the argument that g^{000} and g^{001} are of the same order of magnitude, in agreement with the calculations of Brennan *et al.* This implies that the main body of the discharge, where the diffusion flux is small compared with the flux due to drift in the electric field direction, is well described by the zero and first order terms of the gradient expansion. However, in the wings of the distribution, $(1/\lambda_z n)\partial n/\partial z$ may increase to the point where second and higher order terms are required in the 'local' description (Blevin and Kelly 1990). This has important consequences because the need for higher order gradients then requires that higher order transport coefficients appear in the continuity equation. The 'order of magnitude' agreement with the simulations confirms that the terms in the electric field direction are indeed most important in the gradient expansion, implying that energy 'gained' and 'lost' in the electric field direction dominates the description of the local energy distribution function. This is in general agreement with Wedding and Kelly, although in a significantly different configuration where the 'energy exchange axis' is not coincident with the drift axis.

Acknowledgments

The authors gratefully acknowledge the guidance and assistance of Professor H. A. Blevin. This work was funded in part by the Australian Research Council and the Flinders University Research Budget. In addition we acknowledge the partial financial support of Flinders University Research Scholarships.

References

Blevin, H. A., and Fletcher, J. (1984). *Aust. J. Phys.* **37**, 593.
Blevin, H. A., and Kelly, L. J. (1990). *In* 'Nonequilibrium Effects in Ion and Electron Transport' (Eds E. E. Kunhardt and R. J. Van Brunt), pp. 67–81 (Plenum: New York).
Bracewell, R. N., and Riddle, A. C. (1967). *Astrophys. J.* **150**, 427.
Brennan, M. J., and Garvie, A. M. (1990). *Aust. J. Phys.* **43**, 765.
Brennan, M. J., Garvie, A. M., and Kelly, L. J. (1990). *Aust. J. Phys.* **43**, 27.
Brooks, R. A., and Di Chiro, G. (1976). *Phys. Med. Biol.* **21**, 689.
Dean, S. R. (1983). 'The Radon Transform and Some of its Applications' (Wiley: New York).
Garvie, A. M., and Sorell, G. (1990). *Rev. Sci. Instrum.* **61**, 138.
Herman, G. T. (1980). 'Image Reconstruction from Projections: The Fundamentals of Computerized Tomography' (Academic: New York).
Kelly, L. J., Brennan, M. J., and Wedding, A. B. (1989). *Aust. J. Phys.* **42**, 365.
Ohmori, Y., Shimozuma, M., and Tagashira, H. (1988). *J. Phys.* D **21**, 724.
Phelps, A. V., and Pitchford, L. C. (1985). *Phys. Rev.* A **31**, 2932.
Radon, J. (1917). *Ber. Verb. Saechs. Akad. Wiss. Leipzig Math. Phys.* **69**, 262.
Stanton, P. N., and St. John, R. M. (1969). *J. Opt. Soc. Am.* **59**, 252.
Tagashira, H., Taniguchi, T., and Sakai, Y. (1980). *J. Phys.* D **13**, 235.
Vainshtein, B. K. (1971). *Sov. Phys. Dokl.* **16**, 66.
Wedding, A. B., and Kelly, L. J. (1989). *Aust. J. Phys.* **42**, 101.

Manuscript received 4 June, accepted 25 September 1990